Lab on a Chip

Accepted Manuscript

ROYAL SOCIETY OF CHEMISTRY

www.rsc.org/loc

Lab on a Chip

RSCPublishing

ARTICLE

Rapid Determination of Cell Mass and Density using Digitally-Controlled Electric Field in a Microfluidic Chip

Cite this: DOI: 10.1039/x0xx00000x

Received 00th July 2014,
Accepted 00th xxxx 2014

DOI: 10.1039/x0xx00000x

www.rsc.org/

Yuliang Zhao,[a] Hok Sum Sam Lai,[a] Guanglie Zhang,[a*] Gwo-Bin Lee [b] and Wen Jung Li[a*]

The density of a single cell is a fundamental property of cells. Cells in the same cycle phase have similar volume, but the differences in their mass and density could elucidate each cell's physiological state. Here we report a novel technique to rapidly measure the density and mass of a single cell using an optically-induced electrokinetics (OEK) microfluidic platform. Presently, single cellular mass and density measurement devices require complicated fabrication process and their output is not scalable, i.e., it is extremely difficult to measure the mass and density of a large quantity of cells rapidly. The technique reported here operates on a principle combining sedimentation theory, computer vision, and micro particle manipulation techniques in an OEK microfluidic platform. We will show in this paper that this technique enables the measurement of single-cell volume, density, and mass rapidly and accurately, in a repeatable manner. The technique is also scalable -- it allows simultaneous measurement of volume, density, and mass of multiple cells. Essentially, a simple time-controlled projected light pattern is used to illuminate selected area on the OEK microfluidics chip that contains cells to lift the cells to a particular height above the chip's surface. Then, the cells are allowed to "free fall" to the chip's surface, with competing buoyancy, gravitational, and fluidic drag forces acting on the cells. By using a computer vision algorithm to accurately track the motion of the cells and then relate the cells' motion trajectory to sedimentation theory, the volume, mass, and density of each cell can be rapidly determined. A theoretical model of micro-sized spheres settling towards an infinite plane in a microfluidic environment is first derived and validated experimentally using standard micro polystyrene beads to demonstrate the viability and accuracy of this new technique. Next, we show that yeast cell volume, mass, and density could be rapidly determined using this technology, with results comparable to existing method *suspended microchannel resonator*.

Introduction

The mass of a single cell is the most basic physical property indicating cellular metabolic rate and its fate[1], while the density of a single cell reveals more detailed information on the cell state[2,3]. Related to cell physiology, the mass and density of a single cell also reveal the nature of cell cycle regulation[4–6] more closely than indirect parameters such as cellular shape or non-aqueous mass. The measurement of cell mass and density can also provide a direct and effective evaluation mechanism to monitor cell responses to external stimuli such as drugs and environmental changes[3].

Recently, as a tool of proteomics, mass spectrometry utilizing transition element isotopes has been used for cellular mass measurement[7–9]. In addition, interferometric microscopy based on the relationship between the quantitative phase image of a cell and its non-aqueous content, is used to measure the "dry mass" of the cell[2,10]. Although these two methods can measure cellular mass in an indirect way, both are restricted by their complicated mapping processes and losses in density information.

Another technique to determine cell mass is using a suspended micro-channel resonator (SMR)[11], which is a cantilever resonator[12,13] integrated in a microchannel, and can be used as a density sensor. A research group led by S. R. Manalis has done tremendous research work in the past decade using this method to measure the density of a single cell[14–16]. The cell mass is obtained by calculating the cell volume using the resistive pulse (Coulter) technique, or by passing the cell through two different kinds of mediums in the SMR[17]. Because of the complicated fabrication process involved, and cells must be captured and passed through the resonators, this technology is less practical when the mass of many cells need to be determined simultaneously. More recently, a pedestal resonant sensor (PRS)[18–20] has been developed by another excellent research group led by R. Bashir with a similar measuring principle. Although it has a lower resolution (10^{-10} g) in the case of mass measurement, however, it is more suitable for measuring adherent cells and effective in measuring the stiffness of a cell[5,19].

On the other hand, the classical and established method of measuring the population density of cells is using density gradient centrifugation[21–23]. During sedimentation, the cells settle to an equilibrium position in a density gradient where they are equivalent to their own natural buoyant density. Combined with their volume, the average mass of the cells can be calculated. However, due to its low accuracy, i.e., the density and mass obtained are averaged values of a group of cells, this technique has not much success in measuring the density and mass of a single cell. Even now, researchers have continued to measure cellular sedimentation velocity[24,25] of cells, rather than single cell density and mass. One reason is that it is difficult for a single cell to settle in the same way repeatedly. Furthermore, taking into account the large variations in the mass and density of cells, the average value of mass from many cells may not provide enough information regarding the true physiology state of a cell. Therefore, the direct, rapid and repeatable measurement for buoyancy mass and density of a single cell is still a technical challenge.

In this paper, we present the possibility of using optically-induced electrokinetics (OEK) as a practical solution to this classical problem. OEK is essentially a dielectrophoresis (DEP) system but it uses digitally-controlled and optical images to define virtual electrodes instead of metal electrodes. The basic principle was first reported by P. Y. Chiou[26] et al. (2005), and has sometimes been referred to as "optoelectronics tweezers". Based on OEK technology, single and parallel manipulation of cells[27] have been reported, including cell transport[28,29], separation[30,31], rotation[32] and patterning[33].

The operation principle and the structure of the OEK chip make it extremely difficult to use a lateral microscope for observing the sedimentation of the cells laterally. In our work, a monocular microscope system placed on top of the OEK chip was adapted to observe cellular sedimentation displacement in the vertical direction. Other researchers have tracked micron-scale and nano-scale particles under a single camera microscope using fluorescent[34] and multiplane[35] methods. We have shown that just by using an image-matching algorithm, we could track the vertical trajectory of micron-scale particles accurately. The defocused images of micro particles at different heights captured by a microscope appeared differently because of the changed diffractive and refractive light paths. Hence, a micro particle's vertical position could be obtained by comparing the particles' time-sequence images captured during its motion trajectory with the static calibrated images captured at known heights, without any change in hardware configuration.

In this paper, we will show that the mass and density of a single cell could be measured utilizing an OEK system and the simple micro-vision technique discussed above. First, the density and mass of micro polystyrene beads were measured to validate the method. Two types of micro beads (radius of 5.26 μm and 10.42 μm) were tested first before experiments on cells were conducted. A high-speed (maximum 48 fps) and high-resolution (1280 × 1024 pixels) camera was used to record the images of the beads at different heights in an OEK chip in a time sequence. To calibrate the height of micro beads from a reference plan, static bead images at different heights from a reference plan were obtained by keeping the bead on the OEK chip's surface, while the objective stage of the microscope was moved vertically. Since the movement of the stage is controlled to an accuracy of 0.1 μm in the vertical direction, the standard images captured by the camera could provide the same vertical displacement resolution if the images are processed appropriately. Hence by comparing the static (calibration) images with images captured from actual experiments, the height of a micro particle as a function of time could be obtained by analyzing the sequence of images captured from a dynamically moving micro particle. And hence, the bead's displacement trajectory, velocity, and acceleration during the sedimentation process inside the OEK chip could be deduced. According to sedimentation theory, the viscous force varies with the distance when micron-sized spherical objects are falling perpendicular to a single, infinite plane. To describe the changing viscosity force, which dominates the sedimentation process, the correction factor to Stokes' Law is required and was also experimentally determined in our work. We will show in the *Results and Discussion* section that the accurate determination of this correction factor will allow the matching of experimental results to classical analytical results for the sedimentary trajectories of the beads and cells in an OEK chip. To demonstrate that this OEK-based cell mass and density measurement technique can be generalized to measure non-spherical cells, we tested yeast cells following the same experimental procedure for the beads. The measurement results of the specific cellular mass and density of 44 individual yeast cells are given in the *Results and Discussion* section. We will show that the density and mass of yeast cells obtained using the OEK-based methods reported here are close to the values reported by others, as compared in the table below.

Table 1 Comparison of yeast cell mass/density measured by the OEK-based method proposed in this paper with the SMR method.

Method	Reference	Density ($g\,ml^{-1}$)	Volume (μm^3)	Buoyant Mass (pg)
SMR	Bryan et al. 2010[14]	1.08-1.13	40-260	4-17
OEK	This paper	1.04-1.13	85-350	6-36

Method

The OEK system

Fig.1 illustrates the OEK system and the geometrical configuration of the OEK chip, which were described in more detail in our prior work related to cancer cell patterning[33] and controlling fluidic interface instability[36]. The microfluidic chamber is constructed from two pieces of indium tin oxide (ITO)-coated glasses (3 cm × 3 cm × 1 mm). The height of the medium (DI water) between them is about 60 μm with a relative permittivity of 80 and a conductivity of 1.3×10^{-2} S m^{-1}. A 1 μm thick layer of hydrogenated amorphous silicon (a-Si:H) is deposited at the bottom ITO glass substrate. When an AC voltage bias is applied between these two ITO layers, no electrical conduction path is formed until a digital image is projected onto the surface of the a-Si:H layer. Since the light image locally increases the electrical conductivity of a-Si:H, virtual electrodes are formed in the illuminated area. In Fig.1, the light spot (in green) controlled by the computer is generated by the projector. After being shrunk by the optical condenser, it passes through the ITO glass and is patterned onto the a-Si:H layer. Compared to the dark area, the green area forms a virtual electrode which polarizes the objects around it, similar to a metal electrode. The polarized micro objects are attracted or repelled by the DEP force generated by the induced non-uniform electric field. While the micro particle on top of the green area is lifted into the fluidic medium, the micro particle that is far from the green electrode will remain on the surface of the OEK chip. Compared to the complicated fabrication processing of traditional DEP and microfluidic techniques, selective manipulation of the micro-objects becomes simple and flexible using the OEK system.

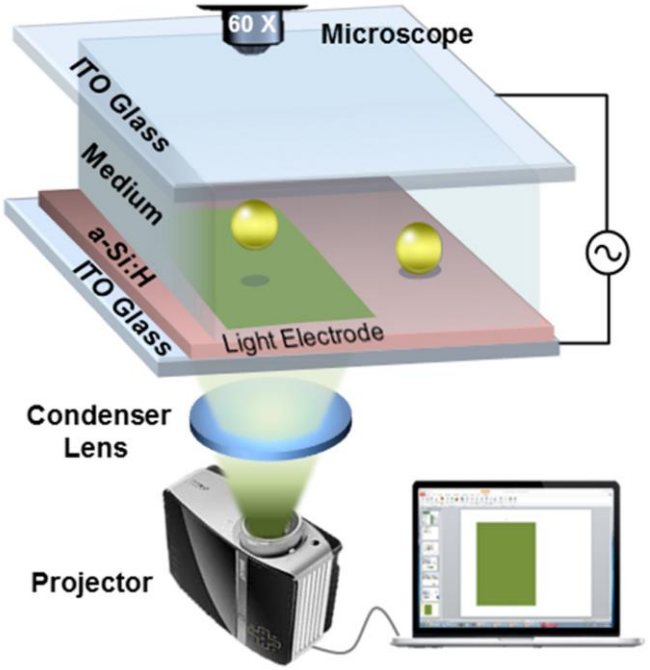

Fig. 1 Illustration of the OEK system and the OEK chip. The experimental system consists of a computer, a signal generator, a display projector, and a microscope; the enlarged illustration of the OEK chip details the different layer structures.

Manipulation of cells and beads under OEK system

When light is projected on a particular area on the photoconductive layer, a localized DEP field is generated across the lighted area of the conductive layer. Assuming that a micro-particle suspended in the medium is perfectly spherical, the time-averaged DEP force acting on the particle in an OEK device can be expressed in as[37]

$$\boldsymbol{F}_{DEP} = 2\pi\varepsilon_m r^3 \mathrm{Re}[\mathcal{K}(\omega)]\nabla|\boldsymbol{E}|^2 \quad (1)$$

where ε_m is the dielectric permittivity of the medium, r is the radius of the particle, $\mathcal{K}(\omega)$ is the Clausius-Mossotti (CM) factor, ω is the applied angular frequency across the medium, and $\boldsymbol{E}$ is the electric field. The CM factor can then be expressed as

$$\mathcal{K}(\omega) = \frac{\varepsilon_p{}^* - \varepsilon_m{}^*}{\varepsilon_p{}^* + 2\varepsilon_m{}^*} \quad (2)$$

where $\varepsilon_i{}^* = \varepsilon_i - j\sigma_i/\omega$, i=p or m, denoting the particles and the medium respectively, and σ is the conductivity. However, a cell commonly consists of a nucleus, cytoplasm, and other organelles and is surrounded by a membrane. It can be considered as a single-shell model instead of a homogeneous sphere. An approximation of the effective complex permittivity of spherical like cells[38] is given by

$$\varepsilon_p{}^* = c_s r\left[\frac{j\omega\tau_c + 1}{j\omega(\tau_s + \tau_c) + 1}\right] \quad (3)$$

where, c_s is the surface capacitance of the membrane, and $\tau_s = c_s r/\sigma_p$ and $\tau_c = \varepsilon_p/\sigma_p$. Based on the particle's dielectric properties, the degree of forces affecting them can be adjusted by controlling the frequency of AC voltage applied across the OEK chip. Fig. 2 illustrates the manipulation of the micro particles under the OEK system and the main forces acting on them in the OEK platform. If the particle is above the center of the electrode and the electrode is large enough, then the edge area of the electrode where the DEP force is not vertical can be ignored. The polarized micro particles will suffer mainly a vertical lift DEP force. By adjusting frequency and voltage magnitude of the electric field applied on the OEK chip, the projected electrode can produce a large enough DEP force to overcome the viscosity drag force and the sedimentation force (i.e., gravity and buoyancy forces) to lift the micro particles to a suitable height.

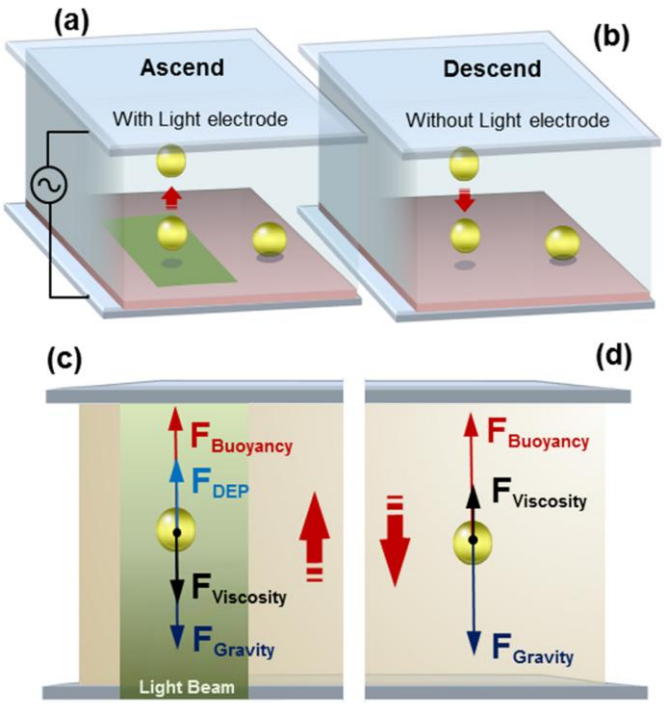

Fig. 2 Illustration of the manipulation of micro particles. (a) When a light beam projected onto the OEK chip, the particle is lifted up and (b) when there is no light projected, the particle starts to sediment. (c) The forces acting on the particle, when it is rising and (d) falling.

Measurement principle of buoyancy mass and density

The principle of manipulating micro particles in an OEK environment has been discussed in the past already by many other researchers[39–41]. Besides the forces mentioned above, forces due to thermal effects, electro-osmosis, Brownian motion, and particle-to-particle interactions can all be neglected under our experimental conditions[23]. These forces have much lower orders of effect (< 10^{-16} N) than the viscosity force, buoyancy force and gravitational force which have orders of magnitude of about 10^{-12} N. The sedimentary force is the resultant effect of the buoyancy and gravitational forces which can be described as

$$F_{Sedimentary} = F_{Gravity} - F_{Buoyancy} = \frac{4}{3}\pi r^3(\rho_{Particle} - \rho_{Medium})\ g \quad (4)$$

where $\rho_{Particle}$ is the density of the particle, ρ_{Medium} is the density of the solution and $\rho_{Particle} - \rho_{Medium}$ is commonly defined as the buoyancy density. Buoyancy mass is the buoyancy density multiplied with the volume. r is the radius of the particle. During sedimentation, the initial vertical state equation of a micro particle (of mass m) can be expressed as

$$m\frac{du}{dt} = F_{Sedimentary} + F_{Viscosity} \quad (5)$$

where u is the vertical velocity of the particle and $F_{Viscosity}$ is the viscosity force exerted by the medium. According to Stokes' Law[43], the equation below can be used to describe the viscosity force acting on a sphere as it moves with velocity u in a medium,

$$F_{\text{Viscosity}} = 6\pi r\eta uK \tag{6}$$

and η is the dynamic viscosity of the fluid medium (at 20 ^{o}C, the viscosity of water[44] of 1.002 is used in our calculations). And, K is the correction factor of Stokes' Law when a sphere is falling perpendicular to an infinitely long plane surface. Then Equation (5) can be expressed as

$$m\frac{du}{dt} = \frac{4}{3}\pi r^3(\rho_{Cell} - \rho_{Medium})\ g + 6\pi r\eta uK \tag{7}$$

The function of the velocity can be solved from Equation (7) as

$$u(t) = \frac{2r^2 g(\rho_{Cell} - \rho_{Medium})}{9\eta K}(1 - e^{-\frac{t}{\tau}}) \tag{8}$$

where $\tau = m/6\pi R\eta K$. Since $\tau \approx 10^{-6}$ seconds, this means that the acceleration time, t, is too fast to be observed and the inertia force can be neglected. So the classical equation for the particle velocity can be simplified as

$$u(t) = \frac{2r^2 g(\rho_{Cell} - \rho_{Medium})}{9\eta K} \tag{9}$$

Then the density of cells can be expressed as

$$\rho_{Cell} = \frac{9\eta Ku}{2r^2 g} + \rho_{Medium} \tag{10}$$

Hence, if the falling velocity u and the correction factor K of Stokes' Law can be obtained, the density of the cell can be calculated using the above equation. Consequently, if the volume of the cell is known, the cell's buoyancy mass can be calculated. However, as the spherical particle is falling perpendicularly towards an infinitely long solid plane, the value of the correction factor K of Stokes' Law will increase, while the sedimentary velocity will decrease. According to Taylor's classical lubrication theory[45], the correction factor K in Stokes' Law is equal to r/h, where h is defined as the gap between the bottom of the falling sphere and the solid plane. That is, as the spherical particle approaches the surface of the plane, $r/h \rightarrow \infty$. Our experimental data shows that if the falling distance of the particle is close to the radius of the particle (about 5~10 μm), and there is no wall around the settling sphere, the correct factor K can be expressed as

$$K = a\frac{r}{h} \tag{11}$$

where a is a constant dictated by the size and density of the sphere. Substituting Equation (11) into Equation (9), then the falling height of the sphere can be modelled as an exponential function of time. After fitting experimental data of the density of known spheres to the height-time function, the constant a can be deduced from the time constant of the exponential function.

Trajectory in the vertical direction

Studies on Depth-from-Defocus (DFD)[46] have been applied in the past in particle tracking with nanometer resolution.[47] In order to minimize the calibration process required for the configuration of the microscope system, an image-matching method is used to obtain the height of the particles suspended in the fluidic medium of the OEK chip. The main idea is to compare the images of the settling particles with standard (static) images of particles of known heights. This method requires more computational complexity, but it enables accurate displacement resolution.

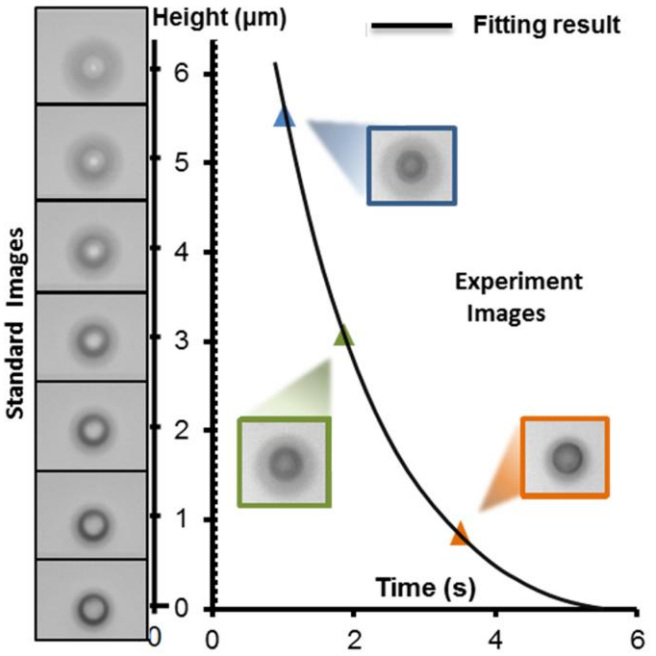

Fig. 3 Illustration of particle height determination by matching the dynamic images with standard images of known heights.

As shown in Fig. 3, the standard images of a bead at different heights are shown on the left side, while the images from a dynamically moving bead is compared to the standard images to determine its trajectory as a function of time. The microscope (NIKON Ti-E) used in our experiments has a stage with 25 nm resolution in the vertical direction. First, the standard (static/calibration) images of a spherical particle are captured at different heights with incremental heights of 0.1 μm. The zero point image (the bottom image in Fig. 3) was selected at the height where the particles have the mostly clear image, i.e., in focus. Then, the manipulation stage of the microscope was moved away from the objective lens at step increments of 0.1 μm. At each incremental step, an image of the particle of interest was obtained. The incremental steps of the manipulation stage were executed by the microscope system automatically. And, the range of the incremental images obtained span from -2 μm below the reference point (zero point image) to 10 μm above reference point. Therefore, there are 121 standard images that are used to compare to time-lapsed images of falling particles to obtain the height of particles in each image frame.

Cell culture

Yeast cells (#20867 obtained from ATCC, USA) were cultured in a shaking incubator (Model KS 4000i, IKA). Yeast Extract Peptone Dextrose Medium (YEPD) with Geneticin 200 mcg ml^{-1} is used as the culture medium. First, 5 – 6 ml of culture medium was added to a 25 cm^2 flask. Then, 200 μl of the prepared suspension solution containing yeast cells was added to the flask. All these steps were performed in a biological safety cabinet (Model HERAcell® 150i, Thermo Scientific). The flask and its contents were kept at the

recommended temperature (28-30 °C) in the incubator with the shaking speed of 220 rpm. The medium was refreshed every two days.

Results and Discussion

Measurement of standard particles

As mentioned earlier, before measuring the density and mass of the cell, standard micro beads with a known density and size are used to calibrate the correction factor of Stokes' Law. Although the function of this correction factor has already been calculated and expressed by many researchers in the past, the actual environment of our experiments is different from those reported work. First, comparing the radii of the particles to the falling distances, researchers have reported either $h \gg r$[48] or $r \gg h$[49,50], while in our experiments the falling distance was kept close to the beads' radius. Second, the radius of the sphere in our experiment was about 5~10 μm, which has not been analyzed in the past. In the low Reynolds number range, most of the experiments in the past mainly focused on the spheres with a millimeter-scale diameter[49–51].

After comparing the time-sequence images of a falling bead with standard images at different heights, the displacement of the bead between any consecutive two image frames can be easily obtained. Combining the elapsed time information recorded in the video (sequence of images), a distance-time plot (*s*-*t* plot) is obtained from the cell sedimentation motion. The *s*-*t* plots are shown in Fig.4.

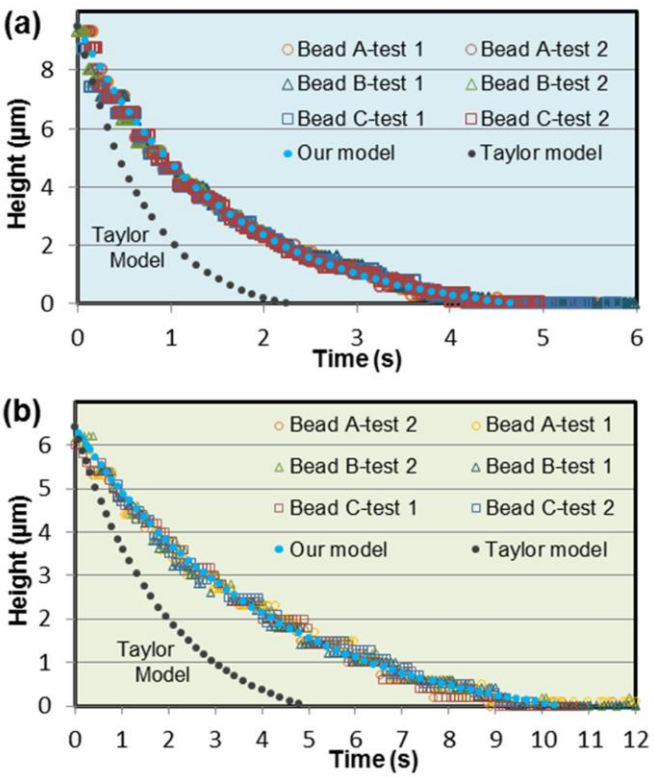

Fig. 4 Time-lapsed height-variation plots of two different kinds of micro beads with radii (a) 10.42 μm and (b) 5.26 μm. Each figure shows experimental data for 3 different polystyrene spheres of the same size, with 2 experiments performed on each sphere. The blue solid dotted lines are the results of curve fitting to Equation (11), with both of them calculated using the same constant a = 2.0. The black dotted lines are the curves calculated from Taylor's classical lubrication theory and marked as Taylor Model.

The entire process of experimentation can be divided into four stages, representing four different motion states of the beads. In the first stage, no light was projected onto the OEK chip, so there was no DEP force acting on the beads, and hence, no displacement change. In stage II, when light was projected, the micro beads were lifted by the DEP force. Different beads were lifted up by different strengths of DEP force, depending on their initial position on the projected image. This ascending phase approximately takes 1~3 s depending on each cell's trajectory. In stage III, the descending phase, the projected light was shut off, i.e., no voltage was applied to the OEK chip, and all the beads fell towards the bottom of the OEK chip. During this sedimentation period, the density and mass of the beads are the crucial factors governing the falling velocity. According to Equations (10), if the density and the radius of beads are the same, they will fall at the same rate. The experimental data shown in Fig. 4 reflects the free-fall motion of the beads which last for 6 s to 12 s during this stage. Finally, after the beads landed on the plane, there was no further displacement; the beads settled down on the bottom of the OEK chip. Therefore, a single cycle for cell-motion image capturing takes about 15 s. In addition, the computational time to process the images for one single cycle takes about 3.5 s. Hence, the approximate time to determine the mass/density of a single cell will take ~18.5 s using the proposed method. As discussed above, the proposed method can be used to measure the density/mass of multiple cells simultaneously -- the quantity of cells measured simultaneously depends on the field-of-view of the microscope and camera used. Our experiment was carried out under a 60× lens, which has a field-of-view that contained at least 100 yeast cells. If a smaller magnification lens and a broader field-of-view camera are used, the quantity of cells whose density and mass could be measured simultaneously could be increased significantly.

So far, to the best of our knowledge, there is no experimental data on obtaining the correction factor K for micron-scale spheres for Stokes' Law. Our method presented above provides a reliable way of measuring the correction factor K for Stokes' Law. Considering that the diameter of the test yeast cell is about 5.5~8.8 μm, the correction factor a = 2.0 was chosen, based on the testing results of similar beads.

Mass and density of Yeast Cells

The sedimentation experiments performed on yeast cells were similar to those performed on micro beads, except that the shapes of most of the yeast cells were ellipsoidal rather than being perfect spheres. Therefore, an additional process is required to make each yeast cell stand "upright" before the cell is lifted up in the fluidic medium. Fig. 5 shows this additional process required for yeast cell experiments.

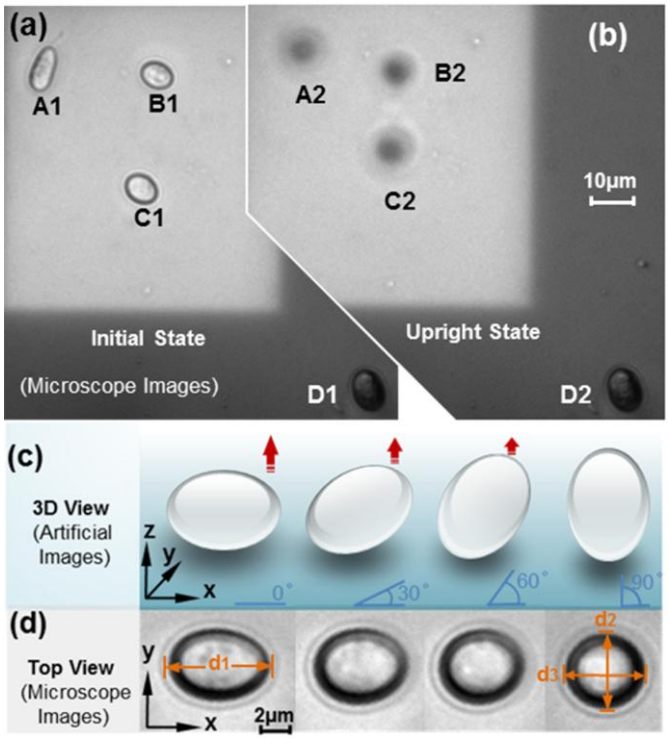

Fig. 5 Microscope images of selective and multiplicative manipulation of yeast cells being lifted up from (a) the initial state to (b) the upright state (i.e., 90° tilt angle). (c) Illustration of the egg-like states of a yeast cell with tilt angles of 0°, 30°, 60° and 90°. (d) Microscope images of the top views of a yeast cell with a tilt angle of 0°, 30°, 60° and 90°, respectively.

The "upright" posture of yeast cells on the chip's bottom surface is required while capturing static images with different heights of the yeast cell. This could be done by adjusting the magnitude of the AC voltage applied cross the chip, i.e., a voltage significant enough to align the cell's orientation to the electric filed lines but not enough to apply enough DEP force to lift the cell. To calculate the volume of the yeast cells, the axes of the ellipsoidal cells were measured in different postures. In Fig. 5(a), A1, B1, C1 are three yeast cells in their initial states while been projected with "optical electrode" image; D1 cell is at a distance away from the electrode. But at this stage no voltage across the OEK chip was applied, so there was no OEK force affecting the A1, B1, and C1 cells. Fig. 5(b) is the image when there is voltage applied across the OEK chip. The three cells on the "optical electrode" are lifted up by the optically-induced DEP force. A2, B2, and C2 show corresponding images of the upright state of the original A1, B1, and C1 yeast cells, respectively. Since the DEP force in the dark area far from the "optical electrode" is small, the orientation of yeast cell D1 is unaffected and hence the image of D2 is similar to D1.

Once the yeast cell was lifted into the fluidic medium to a particular height, the projection light image was turned off, and the yeast cell was allowed to "free fall" in the medium. Since no DEP force acts on the cell any more, gravity force will overcome the buoyant and viscosity forces and dominate the falling process. Fig. 6 shows the details of a yeast cell's falling sequence in the medium inside an OEK chip.

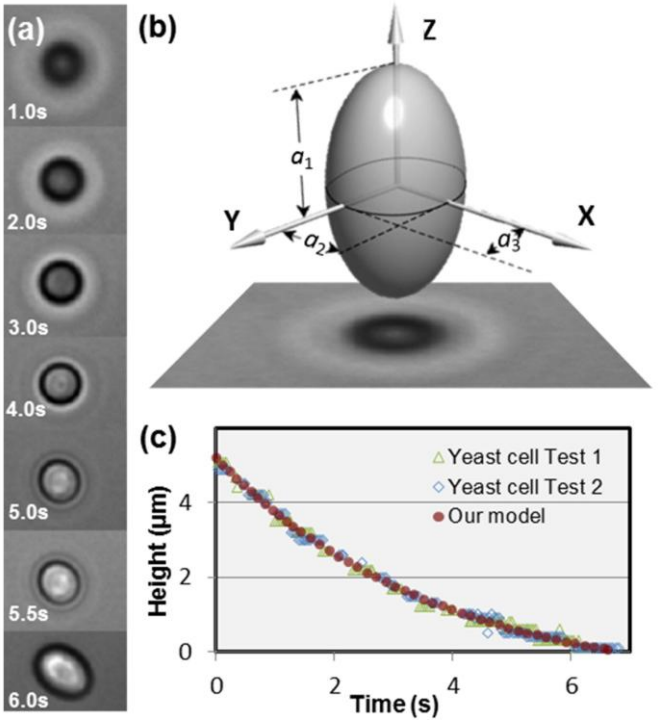

Fig. 6 (a) Microscope image sequence of a yeast cell falling in the medium. (b) Illustration of the relationship between the orientation of the yeast cell and its microscope image while falling. The radius of a1, a2 and a3 are the half of the values of diameters d1, d2 and d3 measured in Fig. 5(d). (c) Repeated test results of one cell's time-lapsed height-variation.

For an ellipsoid[52] moving lengthwise in the medium, the translational friction factor f can be described as: $f=4\pi\eta a_1/(\ln(2a_1/a_2)-0.5)$ where a_1 is the longest semi-axis and a_2 is the shortest semi-axis. This expression is only valid when $a_1^2 \gg a_2^2$, while, in reality, the shortest axis of most of the yeast cells are, at the maximum, 25% shorter than the longest one. The shapes of the yeast cells are closer to being spherical, so an adjusted radius is used, i.e., $r = \sqrt[3]{a_1 a_2 a_3}$.

Using the method described above, measurements for density and mass of 44 single yeast cells were performed (results shown in Fig. 7). The densities of yeast cells varied between 1.04 and 1.13 g cm^{-3}, while the buoyancy mass were in the range of 6~36 pg. This result broadly conforms to those of J. Lee[11] and A. K. Bryan[14]. Considering the differences in cell culturing methods, experimental medium types, cell cycle synchronicity and other conditions, these results demonstrate that our method is practical for measuring the density and mass of a single cell.

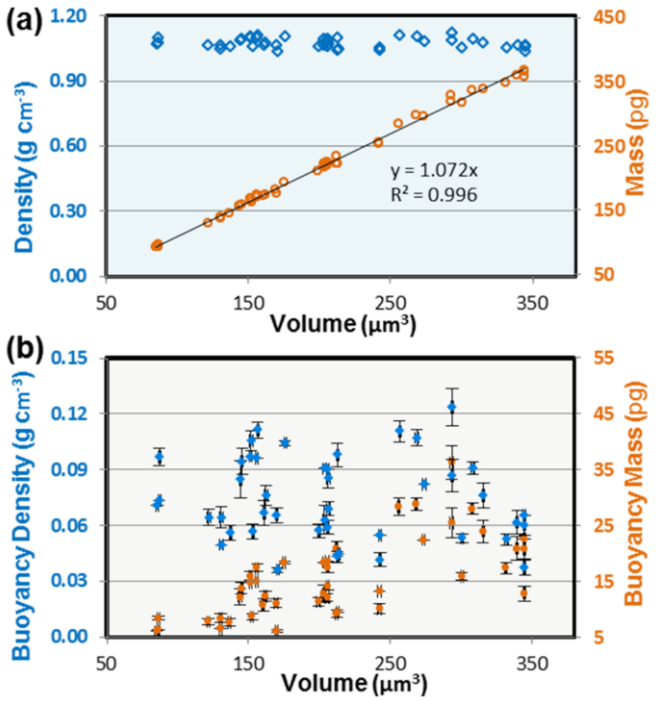

Fig. 7 The measured results of (a) densities, mass and volume and (b) buoyance density (difference between cell density and medium density) and buoyance mass (buoyance density multiply cell volume) of 44 individual yeast cells.

All the data points in Fig. 7(b) are averaged values from 2~5 times of experiments (where the motion of multiple yeast cells were tracked) under the same conditions. The average deviation is 5.2%. The key error source could come from the displacement measurement error caused the determination of motion trajectory of each cell using a computational algorithm in analyzing captured time-sequenced images. The brightness difference between images and random noises produced by the projector, CCD and other components of the image acquisition system could all contribute to the measurement error. In addition, in the non-uniform electrical field, cellular shape and size could change after prolonged polarization which could induce error in determining the cells' settling velocities.

Conclusions

A rapid single cell density and mass determination method has been developed by combining computer vision, micro particle manipulating, and sedimentation theory in an OEK microfluidic platform. This method is characterized for measuring micro particle's buoyancy mass and buoyancy density based on the classical buoyancy density sedimentation principle. The micro particles and cells could be lifted up by digitally-controlled DEP force in the medium of the OEK chip, and then allowed to "free fall" to the OEK chip's surface. Utilizing an image processing technique, the falling motion of the cells/micro beads could be tracked from sequential images frames. Based on the sedimentation theory of micro particles in solution, we successfully implemented a sedimentation velocity detection scheme to measure buoyant density and mass of micro particles and yeast cells. We envision that this new method could potentially be widely used for determining the density and mass of many types of cells rapidly.

Acknowledgements

The authors gratefully acknowledge supports from Hong Kong Research Grants Council (Project no: CityU 118513 and 125513), Chinese Academy of Sciences - Croucher Funding Scheme for Joint Laboratories (Project no: 9500011) and Nanshan core technology breakthrough project: KC2013JSJS0003A. The authors would like to thank Dr. Fei Fei, Dr. Zhikun Zhan, and Mr. Yi Li, all at the City University of Hong Kong, for their insightful discussions on this research project.

Notes and references

[a] Dept. of Mechanical and Biomedical Engineering, City University of Hong Kong, Hong Kong.

[b] Dept. of Power Mechanical Engineering, National Tsing Hua University, Hsinchu 30013, Taiwan.

1. M. Godin, F. F. Delgado, S. Son, W. H. Grover, A. K. Bryan, A. Tzur, P. Jorgensen, K. Payer, A. D. Grossman, M. W. Kirschner, and S. R. Manalis, *Nat. Methods*, 2010, **7**, 387–90.
2. M. Mir, Z. Wang, Z. Shen, M. Bednarz, R. Bashir, I. Golding, S. G. Prasanth, and G. Popescu, *Proc. Natl. Acad. Sci. U. S. A.*, 2011, **108**, 13124–9.
3. W. H. Grover, A. K. Bryan, M. Diez-Silva, S. Suresh, J. M. Higgins, and S. R. Manalis, *Proc. Natl. Acad. Sci. U. S. A.*, 2011, **108**, 10992–6.
4. W. Baldwin and H. Kubitschek, *J. Bacteriol.*, 1984.
5. K. Park, L. J. Millet, N. Kim, H. Li, X. Jin, G. Popescu, N. R. Aluru, K. J. Hsia, and R. Bashir, *Proc. Natl. Acad. Sci. U. S. A.*, 2010, **107**, 20691–6.
6. S. Son, A. Tzur, Y. Weng, P. Jorgensen, J. Kim, M. W. Kirschner, and S. R. Manalis, *Nat. Methods*, 2012, **9**, 910–2.
7. R. Aebersold and M. Mann, *Nature*, 2003, **422**, 198–207.
8. S. C. Bendall, E. F. Simonds, P. Qiu, E. D. Amir, P. O. Krutzik, R. Finck, R. V Bruggner, R. Melamed, A. Trejo, O. I. Ornatsky, R. S. Balderas, S. K. Plevritis, K. Sachs, D. Pe'er, S. D. Tanner, and G. P. Nolan, *Science*, 2011, **332**, 687–96.
9. G. K. Behbehani, S. C. Bendall, M. R. Clutter, W. J. Fantl, and G. P. Nolan, *Cytometry. A*, 2012, **81**, 552–66.
10. G. Popescu, Y. Park, N. Lue, C. Best-Popescu, L. Deflores, R. R. Dasari, M. S. Feld, and K. Badizadegan, *Am. J. Physiol. Cell Physiol.*, 2008, **295**, C538–44.
11. J. Lee, R. Chunara, W. Shen, K. Payer, K. Babcock, T. P. Burg, and S. R. Manalis, *Lab Chip*, 2011, **11**, 645–51.
12. T.-I. Yin, Y. Zhao, J. Horak, H. Bakirci, H.-H. Liao, H.-H. Tsai, Y.-Z. Juang, and G. Urban, *Lab Chip*, 2013, **13**, 834–42.
13. M. Khan, S. Schmid, and P. Larsen, *Sensors Actuators B …*, 2013, **185**, 456–461.
14. A. K. Bryan, A. Goranov, A. Amon, and S. R. Manalis, *Proc. Natl. Acad. Sci. U. S. A.*, 2010, **107**, 999–1004.
15. T. P. Burg, M. Godin, S. M. Knudsen, W. Shen, G. Carlson, J. S. Foster, K. Babcock, and S. R. Manalis, *Nature*, 2007, **446**, 1066–9.
16. M. Godin, A. K. Bryan, T. P. Burg, K. Babcock, and S. R. Manalis, *Appl. Phys. Lett.*, 2007, **91**, 123121.
17. A. K. Bryan, V. C. Hecht, W. Shen, K. Payer, W. H. Grover, and S. R. Manalis, *Lab Chip*, 2014, **14**, 569–76.
18. E. Corbin, L. Millet, and K. Keller, *Anal. Chem.*, 2014, **86**, 4864–72.

19. G. Popescu, K. Park, M. Mir, and R. Bashir, *Lab Chip*, 2014, **14**, 646–52.
20. S. Rashid, E. A. Corbin, B. R. Dorvel, L. J. Millet, P. King, W. P. King, and R. Bashir, *Lab Chip*, 2014, **14**, 1401–4.
21. M. Meselson, F. Stahl, and J. Vinograd, *Highwire Press Natl. Acad. Sci.*, 1957, **43**, 581–588.
22. L. Hartwell, *J. Bacteriol.*, 1970, **104**, 1280–1285.
23. D. Maric, I. Maric, and J. L. Barker, *Methods*, 1998, **16**, 247–59.
24. Z. Wang and J. M. Belovich, *Biotechnol. Prog.*, 2010, **26**, 1361–6.
25. L. T. Bach, U. Riebesell, S. Sett, S. Febiri, P. Rzepka, and K. G. Schulz, *Mar. Biol.*, 2012, **159**, 1853–1864.
26. P. Y. Chiou, A. T. Ohta, and M. C. Wu, *Nature*, 2005, **436**, 370–372.
27. S.-B. Huang, M.-H. Wu, Y.-H. Lin, C.-H. Hsieh, C.-L. Yang, H.-C. Lin, C.-P. Tseng, and G.-B. Lee, *Lab Chip*, 2013, **13**, 1371–83.
28. K.-W. Huang, T.-W. Su, A. Ozcan, and P.-Y. Chiou, *Lab Chip*, 2013, **13**, 2278–84.
29. K.-W. Huang, Y.-C. Wu, J.-A. Lee, and P.-Y. Chiou, *Lab Chip*, 2013, **13**, 3721–7.
30. W. Liang, Y. Zhao, L. Liu, Y. Wang, Z. Dong, W. J. Li, G.-B. Lee, X. Xiao, and W. Zhang, *PLoS One*, 2014, **9**, e90827.
31. Y. Zhao, W. Liang, G. Zhang, J. D. Mai, L. Liu, G.-B. Lee, and W. J. Li, *Appl. Phys. Lett.*, 2013, **103**, 183702.
32. L.-H. Chau, W. Liang, F. W. K. Cheung, W. K. Liu, W. J. Li, S.-C. Chen, and G.-B. Lee, *PLoS One*, 2013, **8**, e51577.
33. N. Liu, W. Liang, L. Liu, Y. Wang, J. Mai, G. Lee, and W. Li, *Lab Chip*, 2014, **14**, 1367–1376.
34. M. Wu, J. W. Roberts, and M. Buckley, *Exp. Fluids*, 2005, **38**, 461–465.
35. P. A. Dalgarno, H. I. C. Dalgarno, A. Putoud, R. Lambert, L. Paterson, D. C. Logan, D. P. Towers, R. J. Warburton, and A. H. Greenaway, *Opt. Express*, 2010, **18**, 877–884.
36. F. Wang, H. Yu, N. Liu, J. D. Mai, L. Liu, G.-B. Lee, and W. Jung Li, *Appl. Phys. Lett.*, 2013, **103**, 214101.
37. H. and N. G. G. Morgan and N. G. Green, *AC Electrokinetics: colloids and nanoparticles*, Research Studies Press, 2003.
38. T. B. JONES, *Electromechanics of Particles*, 1995.
39. W. Liang, S. Wang, Z. Dong, G.-B. Lee, and W. J. Li, *Micromachines*, 2012, **3**, 492–508.
40. W. Liang, N. Liu, Z. Dong, L. Liu, J. D. Mai, G.-B. Lee, and W. J. Li, *Sensors Actuators A Phys.*, 2013, **193**, 103–111.
41. N. G. Green, a Ramos, and H. Morgan, *J. Phys. D. Appl. Phys.*, 2000, **33**, 632–641.
42. Y. Zhao, W. Liang, G. Zhang, J. D. Mai, L. Liu, G.-B. Lee, and W. J. Li, *Appl. Phys. Lett.*, 2013, **103**, 183702.
43. Howard Brenner, *J. Fluid Mech.*, 1962, **12**, 35–48.
44. R. Weast, M. Astle, and W. Beyer, *CRC handbook of chemistry and physics*, 1988.
45. R. Cox and H. Brenner, *Chem. Eng. Sci.*, 1967, **22**, 1753–1777.
46. M. Subbarao and G. Surya, *Int. J. Comput. Vis.*, 1994, **13**, 271–294.
47. A. Marki, E. Ermilov, A. Zakrzewicz, A. Koller, T. W. Secomb, and A. R. Pries, *Biomech. Model. Mechanobiol.*, 2013.
48. B. Lin, J. Yu, and S. Rice, *Phys. Rev. E. Stat. Phys. Plasmas. Fluids. Relat. Interdiscip. Topics*, 2000, **62**, 3909–19.
49. a. Ambari, B. Gauthier-Manuel, and E. Guyon, *J. Fluid Mech.*, 1984, **149**, 235–253.
50. J. O. Marston, W. Yong, and S. T. Thoroddsen, *J. Fluid Mech.*, 2010, **655**, 515–526.
51. A. Mongruel and C. Lamriben, *J. Fluid Mech.*, 2010, **661**, 229–238.
52. H. C. Berg, *Random walks in biology*, Princeton University Press, Princeton, 1993.

